Tectonophysics 664 (2015) 98–108

Contents lists available at ScienceDirect

Tectonophysics

journal homepage: www.elsevier.com/locate/tecto

Ultrafine spherical quartz formation during seismic fault slip: Natural and experimental evidence and its implications

Li-Wei Kuo [a,*], Yen-Fang Song [b,**], Che-Ming Yang [a], Sheng-Rong Song [c], Chun-Chieh Wang [b], Jia-Jyun Dong [a], John Suppe [c], Toshihiko Shimamoto [d]

[a] National Central University, Taiwan
[b] National Synchrotron Radiation Research Center, Taiwan
[c] National Taiwan University, Taiwan
[d] State Key Laboratory of Earthquake Dynamics, Institute of Geology, China Earthquake Administration, China

ARTICLE INFO

Article history:
Received 17 March 2015
Received in revised form 20 August 2015
Accepted 1 September 2015
Available online 18 September 2015

Editor: Rob Govers

Keywords:
Ultrafine spherical quartz
Principal slip zone
Chelungpu fault
TCDP
Synchrotron
Pseudotachylyte

ABSTRACT

In recent works on the determination of pseudotachylyte within the principal slip zone (PSZ) of the Chelungpu fault (Taiwan), we demonstrated that frictional melting occurred at shallow depths during the 1999 Mw 7.6 Chi-Chi earthquake. Thus, the characteristics of melts are of paramount importance to investigate processes controlling dynamic fault mechanics during seismic slips. We conducted rock friction experiments on siltstone recovered from the Taiwan Chelungpu fault Drilling Project (TCDP) at a slip rate of 1.3 m/s and a normal stress of 1 MPa. Here we not only target to characterize experimental pseudotachylyte and evaluate the associated frictional behavior, but also compare it with natural frictional melts of TCDP. Our results show that (1) initial shear stress drop was related to the generation of low viscosity melt patches, (2) the evolution of shear stress in the postmelting regime was congruent with frictional melt rheology, and (3) the slip strengthening presumably resulted from the extremely low content of water of the frictional melt. In particular, the state-of-art of in situ synchrotron analyses (X-ray diffraction and Transmission X-ray Microscope) determine the presence of ultrafine spherical quartz (USQ) grains (~10 nm to 50 nm) in the glassy matrices presumably produced at high temperature. Our observations confirm that the USQ grains formed in rock friction experiments do occur in natural faults. We surmise the USQ is the result of frictional melting on siltstone and represents the latest slip zones of the Chelungpu fault, and further infer that the viscous melts may terminate seismic slips at shallow crustal conditions.

1. Introduction

Determination of the physical and chemical processes having occurred during fast fault slips and associated products remains highly challenging due to heterogeneous fault zone properties and geometry. Integration of field geology, rock friction experiments, and theoretical simulation is a way to better address earthquake mechanics (Di Toro et al., 2012; Niemeijer et al., 2012). In particular, with the efforts of rock friction experiments in the last two decades several physical and chemical processes have been suggested to result in coseismic fault lubrication (Tsutsumi and Shimamoto, 1997; Rice, 2006; Di Toro et al., 2004, 2006; Han et al., 2007, 2010; Brantut et al., 2008; Goldsby and Tullis, 2011), but with the exception of frictional melting (pseudotachylyte) evidence for these processes in natural fault zones is scarce (Di Toro et al., 2006). Pseudotachylyte determined both in nature (Sibson, 1975) and rock friction experiments (Spray, 1987; Tsutsumi and Shimamoto, 1997) has been used to infer the seismically natural fault zones, and is allowed to obtain key parameters of the earthquake source (Di Toro et al., 2009). Therefore, the fault mechanics of active faults can be revealed with the presence of the robust seismic indicators such as pseudotachylyte.

The Chelungpu thrust fault was northward ruptured ~90 km as a result of the Mw 7.6 Chi-Chi earthquake which struck central Taiwan on 21st September 1999 (Fig. 1a) (Lee et al., 2001; Ma et al., 2000). After the 1999 Chi-Chi earthquake, the urgent need for investigating the catastrophically active fault drove the initiation of Taiwan Chelungpu fault Drilling Project (TCDP). TCDP was conducted in 2005 and drilled two holes to a depth of 2003 m for Hole-A (Fig. 1b) and 1353 m for Hole-B. Currently, on the basis of continuous coring (Sone et al., 2007; Song et al., 2007a; Yeh et al., 2007), a suite of geophysical measurements (Hirono et al., 2008a; Hung et al., 2007; Wu et al., 2007, 2008), microstructural observation (Boullier et al., 2009; Ma et al., 2006), mineral anomalies (Chou et al., 2012a,b; Hirono et al., 2008b; Kuo et al., 2009, 2011), chemical composition and physical parameters (Hirono et al., 2006a,b; Ishikawa et al., 2008; Kano et al., 2006; Mishima et al., 2006, 2009; Mizoguchi et al., 2008), the active fault zone of the

* Corresponding author at: No. 300, JhongDa Rd., Jhongli District, Taoyuan City 32001, Taiwan.
** Co-corresponding author at: 101 Hsin-Ann Road, Hsinchu Science Park, Hsinchu 30076, Taiwan.
E-mail addresses: liweikuo@ncu.edu.tw, liweikuo@gmail.com (L.-W. Kuo).

http://dx.doi.org/10.1016/j.tecto.2015.09.008
0040-1951/

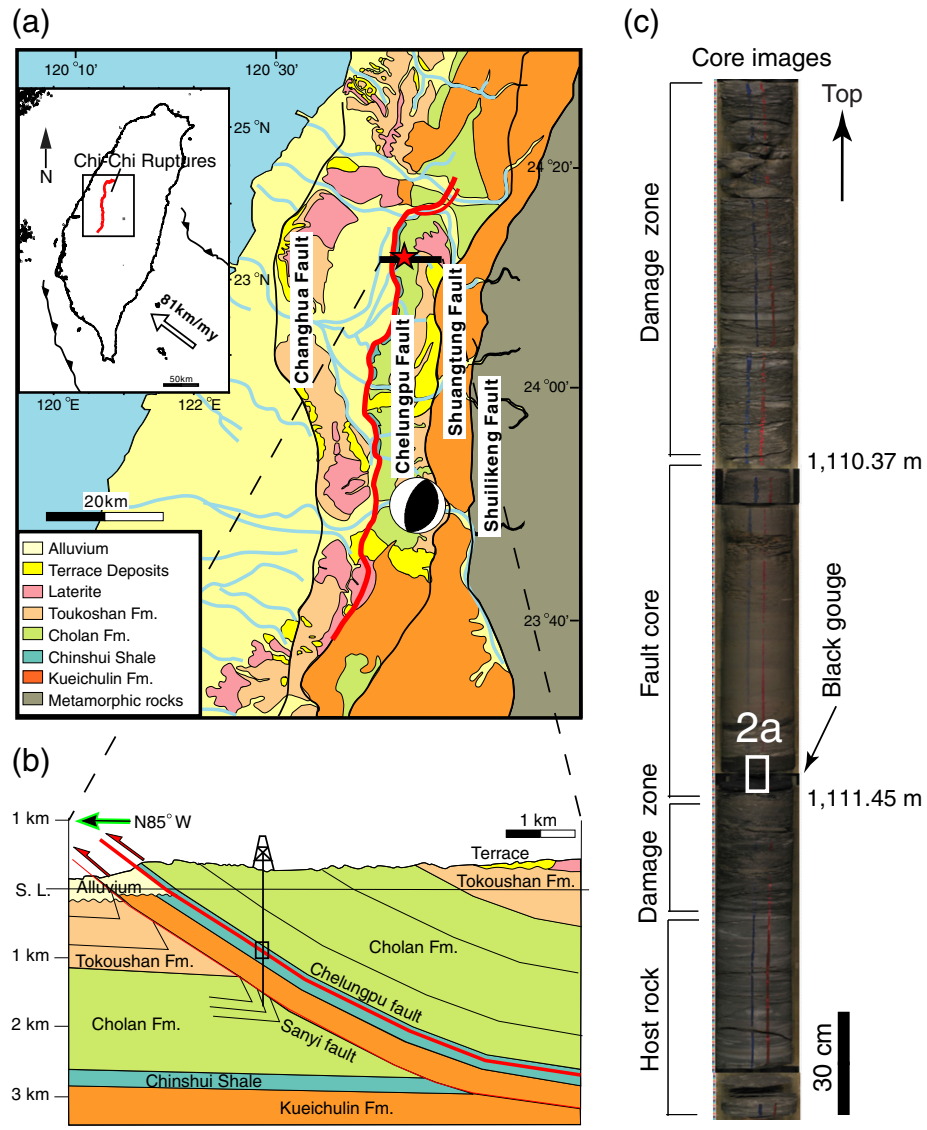

Fig. 1. Geological setting of the 1999 Mw 7.6 Chi-Chi earthquake and location of the TCDP-A drilling site. (a) Location of the TCDP-A drilling site and the 90-km-long surface ruptures associated with the Mw 7.6 earthquake at the central part of western Taiwan. The TCDP site is indicated by a red star. The focal mechanism of the Chi-Chi main shock is located at the hypocenter of the Chi-Chi earthquake. The insert box is the tectonic setting of Taiwan. (b) An E–W cross section of the TCDP-A showing the Chelungpu fault zone and surrounding formations encountered in the borehole (after Hung et al., 2007). The rectangle displaying the principal slip zone active during the 1999 mainshock was identified in the borehole at 1111.29 m depth and the images of fault core samples of the TCDP-A were enlarged in the right panel as (c). (C) The image exhibiting major portions of the Chelungpu-fault along the borehole of TCDP.

Chelungpu fault corresponding to the 1999 at the depth of 1111 m (described as FZ1111 hereafter) in Hole-A (Fig. 1c) and 1137 m in Hole-B.

Boullier et al. (2009) determined the Chi-Chi principal slip zone (PSZ) as a ca 2 cm thick isotropic layer in which the pseudotachylyte-bearing layer is included. Kuo et al. (2009) presented the evidence of frictional melting within the PSZ of FZ1111: (1) lower clay content than surrounding rocks; (2) thermal decomposition of illite, chlorite and kaolinite, and enrichment of smectite; and (3) amorphous materials resulting from transient frictional heating, and suggested that pseudotachylyte was generated and transferred to smectite with hot fluid during the 1999 Chi-Chi earthquake. In addition, on the basis of the determination of pseudotachylyte within the PSZ of the Chelungpu fault, the key parameters related to the earthquake source were obtained such as (1) the temperature (900 °C to 1100 °C) generated during fast fault slips (Kuo et al., 2011), and (2) the localized interval of pseudotachylyte (1 mm) and associated surface fracture energy (Fig. 2a in Kuo et al., 2014a). Recently, rock friction experiments show that frictional melting does occur in clayey gouge during seismic fault slips (Han et al., 2014). Microstructures of the PSZ of TCDP show the transformation from pseudotachylyte to smectite (Janssen et al., 2014). Integrated with natural observation of TCDP and laboratory rock experiments mentioned above, we surmise that pseudotachylyte was generated at shallow depths and promptly altered to smectite in the Chelungpu fault.

In particular, ultrafine spherical quartz (USQ) grains ranging from 50 nm to sub-microns in sizes and pyrite aggregates were obtained from pseudotachylyte within the PSZ of TCDP Hole-A (Fig. 2b and c, and also see Fig. 2b in Ma et al., 2006; see Supporting information Audio S1 for the 3D tomography of Chi-Chi PSZ constructed by TXM). Results of high-velocity friction experiments on clayey gouge show that clay minerals were melted by flash heating at asperities, but USQ was not observed (Han et al., 2014). Results of milling experiments on siltstone of TCDP display that ultrafine particles covered by amorphous surface layers can be generated by comminution (up to 6 h) and fit the mineral anomalies of the PSZ obtained in Hole-B (Hirono et al., 2014). However, the combination of pseudotachylyte with clay anomalies, clay-clast aggregates (CCAs), vesicles, and USQ observed within the Chi-Chi PSZ (Boullier et al., 2009; Kuo et al., 2009, 2011; Ma et al.,

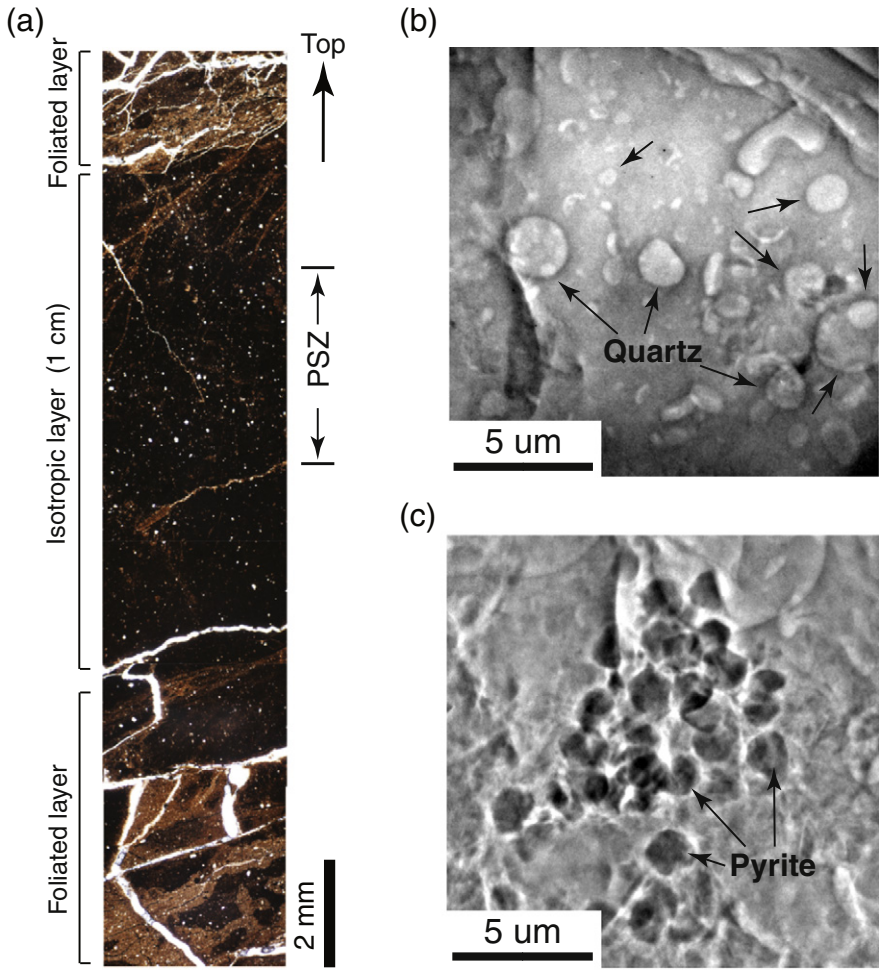

Fig. 2. Microstructural observation of black gouge hosting the Chi-Chi PSZ from TCDP-A. (a) The scan of the thin section of black gouge indicating the PSZ. (b–c) TXM images of the PSZ contains ultrafine spherical quartz in pseudotachylyte shown in b, and pyrite aggregates shown in c.

2006) seems unlikely to be interpreted as the consequence of either long time comminution or flash heating at asperities, and other evidence and the associated mechanism for seismic slips must be identified.

Considering the fault-zone heterogeneity and/or asperity, both fault gouge and surrounding bare rocks could be potential sources to compose the Chi-Chi PSZ during faulting. Since the rock friction experiments on fault gouge could not fully interpret the characteristics of the Chi-Chi PSZ, it suggests that the composition of the active fault zone might be partially derived from the deformation on bare rocks during coseismic slips. Therefore, in an effort to understand fault processes during fast fault slips at shallow depths, we conducted rock friction experiments on siltstone recovered from TCDP (the wall rocks surrounding the PSZ) at a slip rate of 1.3 m/s and a normal stress of 1 MPa. We examined the mineralogy and the macro- and micro-structures of the simulated fault rocks, integrated with the one of the PSZ of TCDP, address the dynamic frictional behavior, discuss possible signatures for determining the PSZ and, by extension, other exhumed fault zones hosted in sedimentary rocks.

2. High-velocity rock friction experiment and analytical methods

2.1. High-velocity rock friction experiment (HVRFE)

The specimens were made of siltstone recovered at a depth of ~1000 m, and the geometry of specimens is a pair of solid cylinders with an outer diameter of 24.8 mm (Fig. 3a). We conducted rock friction experiments with a rotary shear, high-velocity frictional testing apparatus at the National Central University (see Yang et al., 2014 for the details of the machine and sample preparation). All the rock friction experiments reported here were conducted at a normal stress of 1 MPa, at an equivalent slip rate (V) of 1.3 m/s (see Han et al., 2007 for the details of equivalent slip rates), and at room temperature and room humidity. Before we started each friction test, the rotary cylinder of the pair of specimens loaded in the testing apparatus was rotated at a low slip rate (0.03–0.05 m/s) and under low normal stress (up to 0.5 MPa) until the sliding surfaces of both cylinders had become as perfectly parallel as possible. We calculated mechanical data from the raw output data, specimen size, and data-sampling rate (see Hirose and Shimamoto, 2005 for the details of data processing). All our mechanical data are comparable to those of previous HVRFE experiments.

2.2. Scanning electron microscope with energy dispersive spectrometer (SEM/EDX)

To obtain information of the surface texture of frictional melts and its semi-quantitative chemical composition generated by HVRFE, we used FEI QUANTA 200F scanning electron microscope coupled to an energy dispersive spectrometer (SEM/EDX) quantitative analysis at 10 kV with the standardized processes at the National Taiwan University.

2.3. Micro-Raman spectroscopy

To determine if water was present in the pseudotachylyte, we analyzed frictional melts by micro-Raman spectroscopy, and focused on

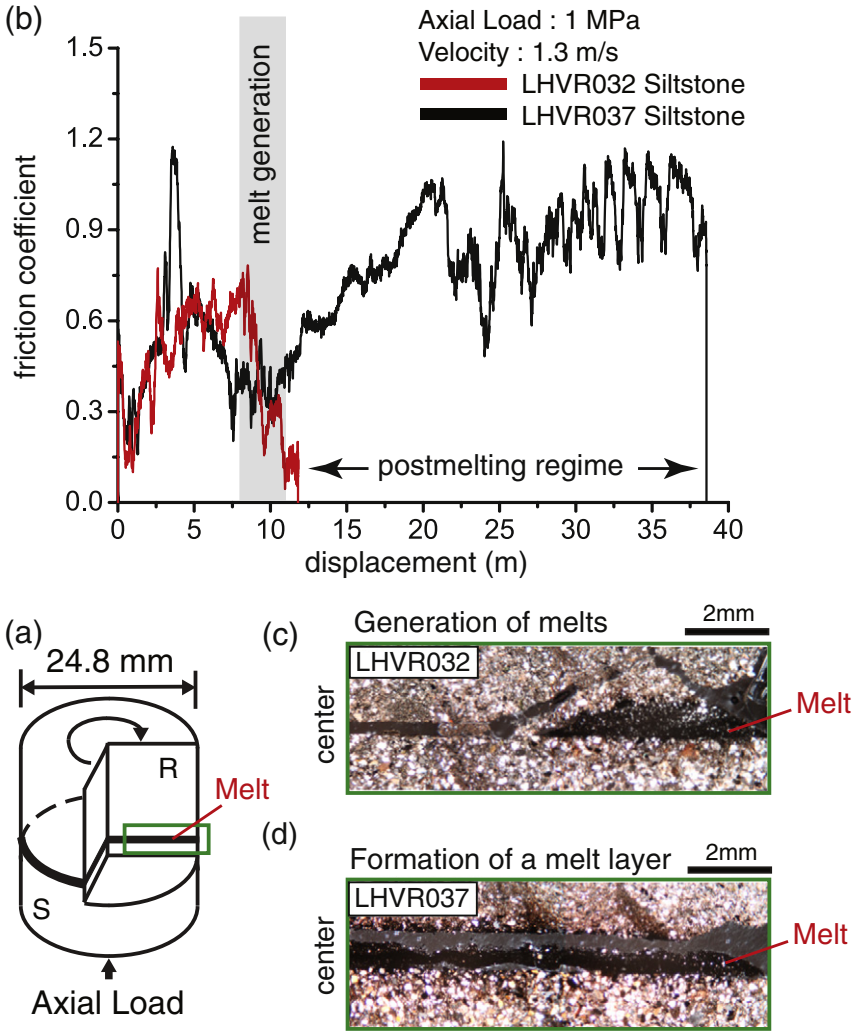

Fig. 3. A specimen assembly for HVRFE and experimental results at a slip rate of 1.3 m/s and a normal stress of 1 MPa. (a) Schematic sketch showing geometry of HVRFE, and a pair of solid cylindrical specimens on siltstone was prepared. (b) Effective coefficient of friction (the ration of shear to normal stress) versus displacement. The gray rectangle denotes the onset of frictional melts. (c–d) A thin section of siltstone after the HVRFE at displacement of 11.8 m shown in c and 38.5 m shown in d, respectively.

the 100–4000 cm^{-1} region of Raman spectrum. The Raman spectra were directly measured on frictional melts with a Horiba Jobin Yvon UV–VIS Labram HR micro-Raman spectroscopy at the National Taiwan Museum. A 532 nm laser was used as the excitation source and beam size was 1–2 μm with a ×100 objective, with a final laser power of 100 mW at sample surface. A microscope was used to focus the excitation laser beam on the analyzed sample (glass plus ultrafine particles) and to collect the backscattered Raman signal with a charge-coupled device (CCD) detector. Acquisition time was 15 s and 5 spectra were measured for each sample.

2.4. Transmission electron microscope (TEM)

Transmission electron microscope produced by FEI Company (TECNAI G2) at the National Taiwan University was performed to retrieve information of ultrafine quartz grains and the associated selected area diffraction pattern (SADP) in experimental products by HVRFE.

2.5. In situ synchrotron transmission X-ray microscopy (TXM)

We collected samples from both siltstone and pseudotachylyte, impregnated those with resin, and cut into about 20 μm thick sections for TXM observation. The TXM facility (Yin et al., 2006) of beamline BL01B (Song et al., 2007a,b) at the National Synchrotron Radiation Research Center (NSRRC) in Taiwan provides 2D micrograph and 3D tomography at spatial resolutions of 50 nm, with first-order diffraction of a Fresnel zone plate at an X-ray energy of 8 keV. The field of view of the image is 15 × 15 $μm^2$ for the first-order diffraction of the zone plate. The phase term can be retrieved by the Zernike's phase contrast method that the morphology was obtained from the change of density contrast in analyzed materials. The gold phase ring is positioned at the back focal plane of the objective zone-plate retards or advances the phase of the zeroth order diffraction by π/2 resulting a recording of the phase contrast images at the detector. A millimeter-scale field of view of the sample can be generated by stitching images from a series of observed positions. After acquiring a series of 2D micrographs with the sample rotated stepwise azimuthally, the 3D tomography data sets were reconstructed by applying a filtered back-projection algorithm based on 181 sequential image frames taken with the azimuth angle rotating from −90° to +90°. The final 3D tomography structures were generated using Amira 3D software to enhance the visualization.

2.6. In situ synchrotron X-ray diffractometer (XRD)

To characterize mineral assemblages of frictional melts, all cylindrical samples sandwiched melts were examined by in situ synchrotron XRD analysis. The in situ X-ray powder diffraction was performed at the XRD end-station of beamline BL01C2 of the NSRRC in Taiwan to

investigate the in situ mineral assemblage in different parts of experimental products by HVRFE (Kuo et al., 2014b). The synchrotron X-ray radiation was generated from the superconducting wavelength shifted magnet of 5.0 T with ring energy of 1.5 GeV typical ring current of 200 to 120 mA. The X-ray wavelength was 0.774908 Å which was delivered by a double crystal monochromator with two Si (111) crystals. The frictional melt was selectively analyzed with the beam size of 500 μm diameter during the X-ray measurement. Two dimensional powder X-ray diffraction patterns were recorded by using Mar345 imaging plate detector with the pixel size of 100 μm and the typical exposure time of 60 s. The one dimensional XRD profile was converted using FIT2D program of a cake type integration.

3. Results

3.1. Frictional evolution in the postmelting regime

The study targets to evaluate the mechanical response of pseudotachylyte derived from sedimentary rocks during fast fault slips at shallow crust conditions in comparison with the observation of TCDP investigated to date (Kuo et al., 2009, 2011, 2014a). To this end, fresh siltstone core retrieved from TCDP was collected, as it is a presumable source rock, surrounding the PSZ of 1999 Chi-Chi earthquake. The average mineral assemblage of siltstone samples utilized in this study contains about 50 wt.% quartz, 10 wt.% plagioclase, 3 wt.% carbonate, 0.5 wt.% pyrite, and 36.5 wt.% clay minerals (see Kuo et al., 2009 for the details of clay mineral assemblages). We manually terminated experiments when frictional melts were generated (a displacement of 11.8 m and 38.5 m in this case).

Initially, the shear stress increased up to a peak value, and then decreased with displacement (described as the peak friction hereafter) (Fig. 3b). In the beginning of the peak friction wear materials (powders) were extruded from the slip surface, and then followed with melt patches generated on the slip surface in the late stage of the peak friction (Fig. 3c). After the peak friction, shear stress progressively increased with displacement and appeared to regularly oscillate to the end (Fig. 3b). The experimental data and optical images show that the frictional melt layer was developed during the slip strengthening (described as postmelting regime hereafter). It suggests that the frictional evolution in the postmelting regime was likely related to the generation of a melt layer (Fig. 3b–d). Apparent coefficient of friction was calculated by the ratio of shear stress to normal stress during the HVRFE. The values of friction coefficient of peak friction were increased from 0.2 to ~0.7, and then decreased to ~0.2 (Fig. 3b). However, the friction coefficient during the postmelting regime increased from 0.2 to 1.0 and oscillated until the end of the experiment (Fig. 3b). In particular, the frictional behavior after the onset of a melt layer is similar to that inferred for argillite (Ujiie et al., 2009), instead of those previous HVRFE on crystalline rocks (Di Toro et al., 2006; Hirose and Shimamoto, 2005; Tsutsumi and Shimamoto, 1997). Because the frictional melt layer was developed during the slip strengthening stage, we suggest that apparent coefficient of friction in the postmelting regime is as the mechanical response of the melt layer controlled by frictional melt rheology.

3.2. Microstructures and chemistry of frictional melts

The experimental slip zone, by comparing the optical observation of the frictional melts under the microscope (Fig. 3c and d), shows a growth of the melt layer during the postmelting regime: (1) the generation of melts of ~0.6 mm thick was discovered at the edge in the initial postmelting regime (Fig. 3c), and (2) the formation of a melt layer of ~0.5 mm thick was determined along the slip surface after large displacement in the end of the experiment (Fig. 3d). The melts and the melt layer on the slip zone appear to be dark, and contain both vesicles and clasts.

Back-scattered electron (BSE) images show the physical and chemical characteristics of the pseudotachylyte (Fig. 4). The pseudotachylyte contains quartz, very minor amount of feldspar and spherical to ellipsoidal vesicles in the glassy matrix. Quartz and feldspar grains exhibit subangular to sub-rounded margins, and vesicles in the matrix of the pseudotachylyte are ranging from sub-micron to 15 μm in size (Fig. 4a and b). In particular, the vesicles in pseudotachylyte generated at the displacement of 38 m (LHVR037) are more irregular and bigger than that derived from the initial generation of melts (LHVR032) (Fig. 4b). We analyzed only the matrices with SEM/EDX to obtain chemical composition, and adopted an average of 46–64 points as a representative chemical composition of pseudotachylyte (the same analytical condition as that in the study of Kuo et al., 2011). The EDS spectra of matrices from the generation of melts (LHVR032) and the formation of a melt layer (LHVR037) show no clear spatial compositional variation (Table 1). In addition, the chemical composition of the pseudotachylyte matrices is similar to that of clay minerals (Kuo et al., 2012), but is slightly enriched in Si, Al, K, and Ca and absent in Fe.

Micro-Raman spectroscopy was utilized to obtain the information on the presence of water which make great influence on the melt viscosity and associated rheology of frictional melting. We examined the matrices of pseudotachylyte, and integrated those results with the one of pure water and quartz. The Raman spectra of matrices of pesudotachylyte show the presence of quartz and absence of water (or contains very few water that the signal was vey tiny and cannot be separated from background in the Raman spectrum) (Fig. 5).

TXM provides three-dimensional information which clearly shows internal structures of analyzed samples that complements the two-dimensional SEM images. The TXM image of host rock shows that an abundant fine-grained matrix composed of platy clay minerals support rounded to sub-angular clasts (Fig. 6a). Instead, the TXM image of the matrix of pseudotachylyte displays that homogeneous glass supports rounded grains of ~10 nm to 15 μm in size, which is much smaller than those of the surrounding host rock (Fig.6b). The representative shape of grains was shown (Fig. 6c) and was reconstructed by utilizing the FEI Amira 3D software (Fig. 6d) (see Supporting information Audio S2 and S3 for the 3D tomography of experimental pseudotachylyte constructed by TXM). Similarity to the occurrence of the PSZ of TCDP (Fig. 2b), the TXM images suggest that numerous ultrafine spherical quartz grains were suspended in the glassy matrices (Fig. 6c), instead of being aggregates such as pyrites observed in TCDP (Fig. 2c). The TEM image of glassy matrix shows similar occurrence of USQ grains to the TXM images, and also detects the crystallinity of quartz grains, instead of being vesicles (Fig. 6e).

Similarity to the sample preparation for the TXM analysis, we collected impregnated thin sections of experimental products and selectively determined pseudotachylyte and the host rock with in situ synchrotron XRD shown in Fig. 7. The XRD spectra of the host rock were plotted as gray lines, and the ones of pseudotachylyte were drawn as black lines. In situ synchrotron XRD results suggest that the mineral phases of the host rock (siltstone) were composed of quartz, feldspar, calcite, illite chlorite, kaolinite, and pyrite. In contrast to the host rocks, the mineral phases of pseudotachylyte were dominantly composed of quartz, and very few feldspar and calcite. No progressive variation of mineral phases from edge to center of the samples was observed (Fig. 7). In addition, the bump from 15 to 40 of two theta resulted from glass was not observed because the tiny signal of glass was depressed by the high detected intensity of quartz. In general, the mineralogy of the matrices of pseudotachylyte determined by in situ synchrotron XRD is identical to the one of both micro-Raman spectroscopy and TEM.

4. Discussion

4.1. Formation of ultrafine spherical quartz (USQ)

The main question that we address here concerns the natural observation of USQ obtained in the PSZ of the Chelungpu fault (Ma et al.,

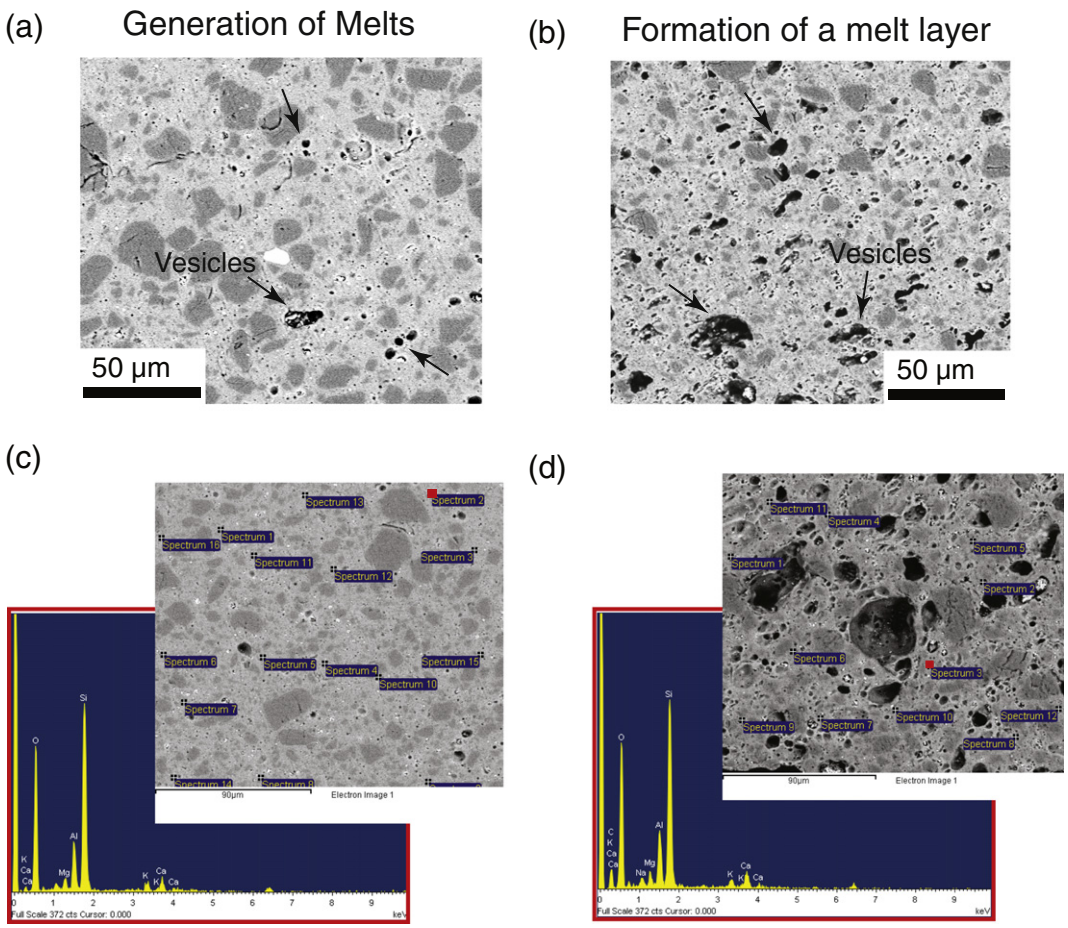

Fig. 4. BSE images of experimental slip zones. (a) The pseudotachylyte formed at displacement of 11.8 m show relatively bright glassy matrix with sub-angular clasts. Spherical and ellipsoidal dark spots are vesicles. (b) The pseudotachylyte formed at displacement of 38.5 m show relatively large irregular vesicles (dark portions) developed in the homogeneous glassy matrix. (c–d) SEM image and EDS analyses of a section of the pseudotachylyte matrix. The location marked in red color showing the representative spectrum below. Note that both the representative spectra of the matrix of the pseudotachylyte are similar (Table 1).

2006). Ultrafine grains in sheared rocks have been previously reported from both field (Chester et al., 2005; Siman-Tov et al., 2013; Viti, 2011; Wilson et al., 2005) and experiments (Han et al., 2010; Hirono et al., 2014; Tisato et al., 2012), but their origin still remains unclear because the limitation of the grain size by a fragmentation process (Griffith cracks) is larger than ~1 μm. Therefore, several physical and chemical processes during faulting were suggested to form ultrafine grains (Han et al., 2007, 2010; Hirono et al., 2014; Koch, 1997). For instance, Han et al. (2007) conducted HVRFE on carbonate rock and found that the thermal decomposition occurred during shear heating and generated ultrafine particles of tens of nanometers in size.

Microstructurally, the USQ grains of TCDP-A were discovered in the aphanitic glassy matrix (Fig. 2a and b) accompanied with numerous vesicles (see Fig. 8 in Kuo et al., 2011) and clayey anomalies (Kuo et al., 2009). It seems that the combination of the characteristics of the USQ was unlikely interpreted as the result of previous mechanisms inferred above. Boutareaud et al. (2010) conducted HVRFE on clayey gouge similar to TCDP gouge at the normal stress of 1.2 MPa and showed the formation of clay clast aggregates. Besides which, Han et al. (2014) conducted HVRFE on clayey gouge at the normal stress of 5 MPa and showed the generation of pseudotachylyte with sub-angular quartz clasts ranged from 1 to 60 μm in size. Neither of them found the USQ grains formed by HVRFE on clay gouge. Instead, the occurrence of our experimental products by HVRFE on siltstone, showing USQ grains in the aphanitic glassy matrix (Fig. 6c) accompanied with numerous vesicles (Fig. 4a and b) and clayey anomalies (Fig. 7), is extremely similar to the natural observation of TCDP-A.

When frictional sliding and melting occurs, preferential melting of the wall rock grains with a high surface-to-area ratio such as the grains are sticking out from the wall rocks into the melt. This process is called Gibbs–Thomson effects (Hirose and Shimamoto, 2003). Three lines of evidences, including (1) micro-Raman spectra indicated that quartz was present in the matrices of pseudotachylyte (Fig. 5); (2) TEM analysis showed nano-scale crystalline grains collected from matrices of pseudotachylyte (Fig. 6e); and (3) in situ synchrotron XRD determined that quartz is the dominant minerals in the pseudotachylyte (Fig. 7), suggest that the ultrafine spherical grains are crystalline quartz. Taken together, it seems to be a reasonable explanation for the formation of

Table 1
Normalized average chemical composition of matrices of pseudotachylyte generated by friction of siltstone with standard deviations.

	[a]n	Na	Mg	Al	Si	K	Ca	Total
LHVR032	46	2 ± 0.45	2.6 ± 0.24	13.6 ± 1.10	66.1 ± 2.33	5.5 ± 0.67	10.2 ± 1.40	100.00
LHVR037	64	2.1 ± 0.49	2.8 ± 0.33	14.2 ± 1.21	64.5 ± 2.20	6.6 ± 0.74	9.8 ± 1.34	100.00

[a]n, number of analyses.

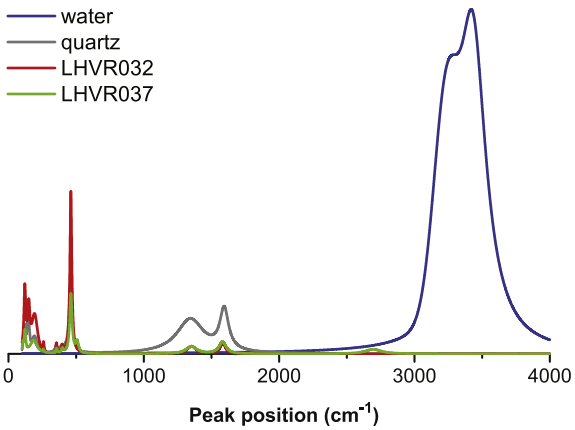

Fig. 5. Representative Raman spectra of the matrices of pseudotachylyte, quartz, and water.

USQ that relatively irregular quartz fragments in the wall rock were reshaped by Gibbs–Thomson effects after frictional melting and thus become smaller and rounded as we observed the USQ grains in the glassy matrices. Therefore, the results of both this and previous studies suggest that the USQ in the PSZ of the Chelungpu fault was plausibly derived from frictional melting on siltstone rather than being generated from clay gouge inferred elsewhere.

4.2. Frictional melt viscosity and frictional evolution during the postmelting regime

The frictional melt generated by HVRFE on siltstone (0.5–0.6 mm) is thicker than the one on crystalline rocks (0.14 mm) (e.g., Hirose and Shimamoto, 2005). In addition, our observation shows that the melt patches are thicker than the surface roughness (Fig. 3c). It seems that solid–solid contacts on the slip surface during experiments are unlikely occurred, and it suggests that melt patches and/or a melt layer may be the main contribution for shear resistance. Here we simply neglect the contribution from solid–solid friction in the central part of the slip surface. Therefore, the frictional melt viscosity and shear strain rate should dominantly contribute to the shear resistance of the simulated fault

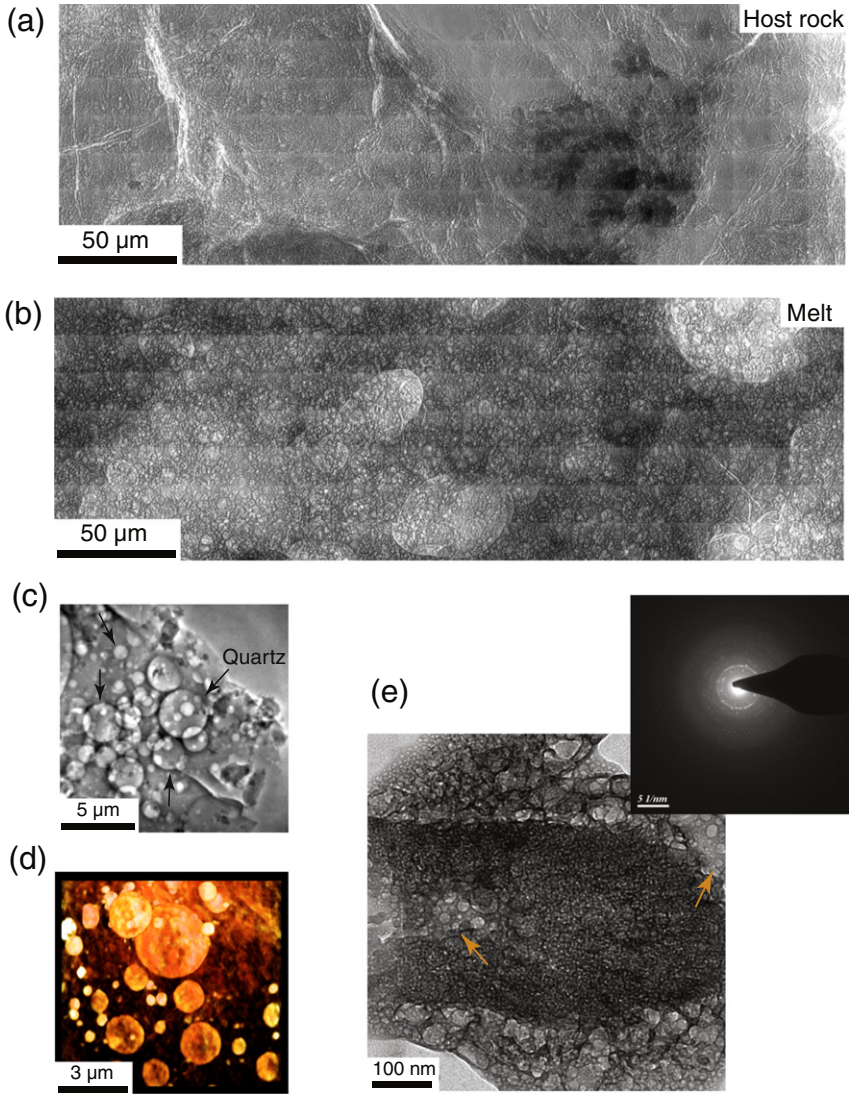

Fig. 6. Internal microstructures of siltstone and experimental pseudotachylyte. (a) TXM image collected from siltstone showing fine clays support sub-angular clasts. (b) TXM image collected from pseudotachylyte matrix showing homogeneous glass surrounds ultrafine spherical quartz. (c) TXM image shows a representative shape of ultrafine spherical quartz. (d) A construction of ultrafine spherical quartz. (e) TEM image displays numerous ultrafine quartz grains in the glassy matrix. SADP shows a diffusion ring presented on the patterns associated with many diffraction spots suggesting the presence of randomly oriented nanoparticles of quartz within an amorphous matrix.

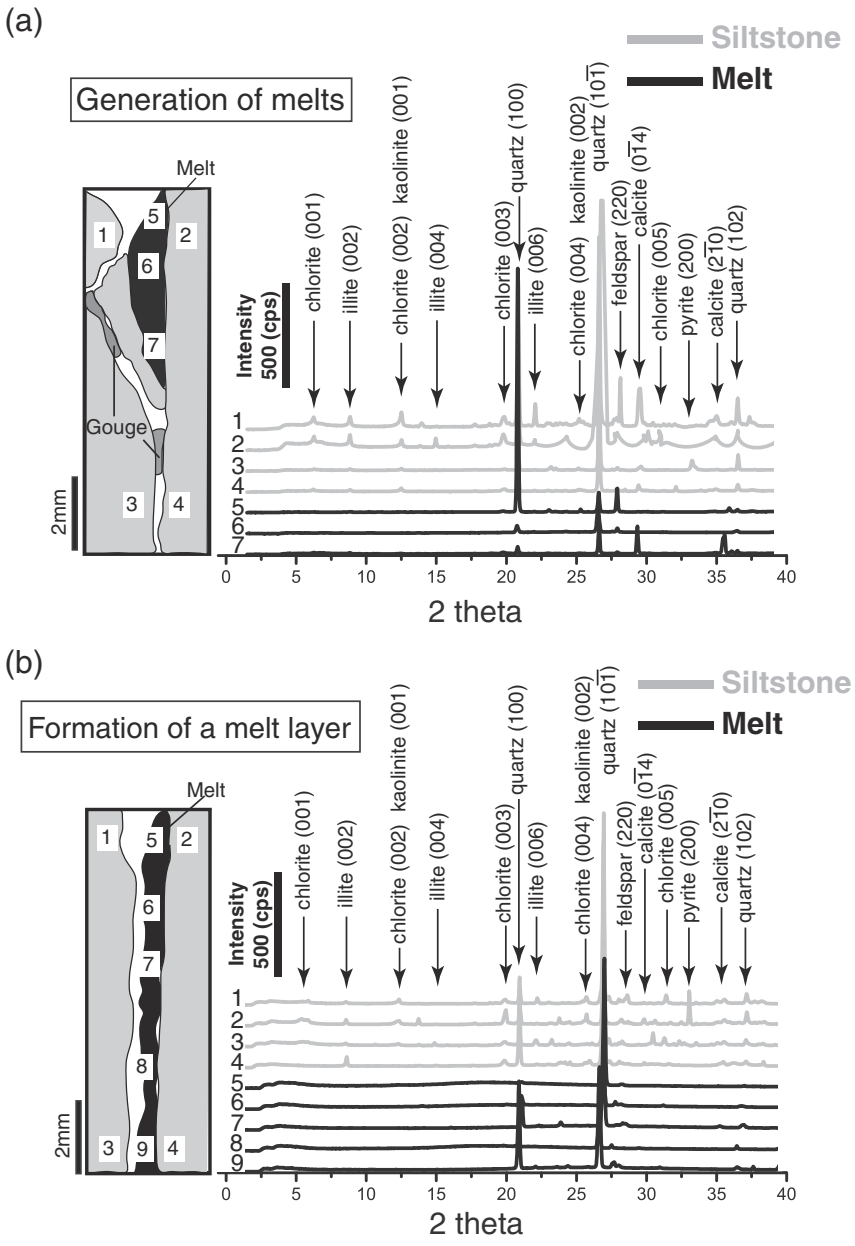

Fig. 7. In situ XRD analysis of experimental products from simulated fault plane. (a–b) Reduced diffraction peak intensity of clay minerals such as illite, chlorite and kaolinite were recognized in the in situ XRD spectra showing no significant variation from the center to the edge as function of temperature for cylindrical sample slid in the slipping plane.

during the postmelting regime, and the associated lubrication approximation is shown as followed.

$$\tau = \eta \frac{dy}{dt} = \eta \frac{V}{w} \quad (1)$$

where τ is the shear stress, η is the apparent viscosity of the melt layer, $d\gamma/dt$ is the strain rate, V is the slip rate, and w is the thickness of the melt layer. Apparent viscosity of frictional melts was calculated by the ratio of the measured shear stress to the shear strain rate (Fig. 8 and Table 2), assuming that the frictional melts behave as a Newtonian fluid. Apparent viscosity increases from ~60 Pa s to 395 Pa s with increasing displacement (solid squares in Fig. 8). The apparent viscosity of the frictional melts is controlled by (1) the volume fraction of solid grains and/or vesicles, and (2) chemical composition in the matrices (Lejeune et al., 1999; Spray, 1993).

For the presence of clasts in the frictional melt layer, we corrected the apparent viscosity with the empirical equation (Kitano et al., 1981) to obtain the associated relative viscosity.

$$\eta_r = \left(1 - \left(\frac{\phi}{A}\right)\right)^{-2} \quad (2)$$

where ϕ is the volume fraction of the solid grains, and A is the parameter related to the packing geometry of the solid grains (2 in our case). To obtain ϕ in the frictional melt layer, we collected BSE images obtained from the center to the edge of the frictional melt layer, estimate ϕ in different places, and then averaged the values. ϕ in the frictional melt layer is ranged from 0.30 to 0.40, and slightly decreases with increasing displacement (Fig. 4). In addition, ϕ in the frictional melt layer is smaller than the one in the host rock (0.55–0.65). Melt viscosity corrected for clasts with the Eq. (2) is ranged from 3 Pa s to 69 Pa s with increasing

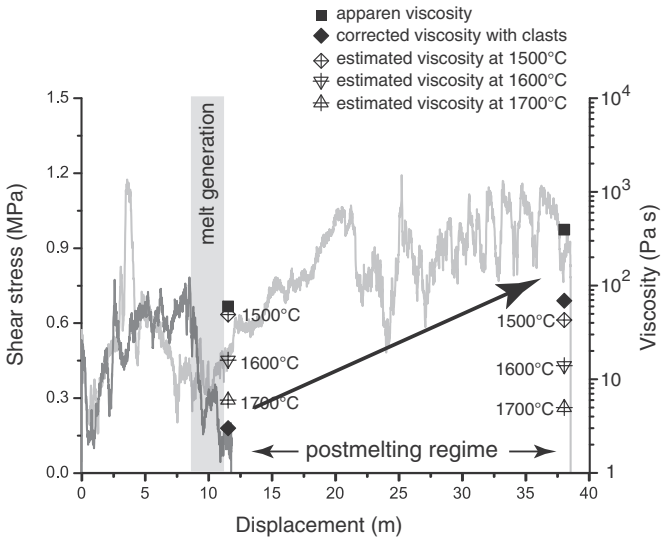

Fig. 8. Plot of the matrix viscosity (open shapes), the viscosity of the melt layer (solid diamond), and the apparent viscosity (solid square) (Table 2). The shear stress versus displacement shown in Fig. 3a is also presented for comparison.

displacement (solid diamonds in Fig. 8 and Table 2). It suggests that the increase of viscosity is unlikely resulted from the increase of volume fraction of solid grains during the postmelting regime. We followed the same procedure as in the case of solid grains to estimate the volume fraction of vesicles in the frictional melts. The ϕ of vesicles was increased from 0.03 to 0.08 with increasing displacement (Fig. 4). Since the volume fraction of vesicles in the frictional melt layer is very small, the contribution of vesicles to the viscosity seems to be negligible (Lejeune et al., 1999). Taken together, the contribution of quartz grains and vesicles is unlikely to result in slip strengthening behavior in the postmelting regime.

From current results we could not obtain the exact chemical composition of frictional melts including the volatile content and water content which has important consequences on the melt viscosity. Therefore, for the consideration of chemical variation in the matrix during the postmelting regime, we simply calculated matrix viscosity with the empirical equation (Fluegel et al., 2004) by inputting the chemical composition data of the matrices (Table 1) and melting temperatures. The in situ synchrotron XRD analyses show that all clay minerals and feldspar disappeared and some quartz partially melted in the products (Fig. 7). It means that the melting temperature is higher than the melting point of illite (1100 °C) and feldspar (1400 °C), and may achieve the melting point of quartz (1700 °C) in the frictional melt layer during experiments (e.g., Lin and Shimamoto, 1998). However, the heterogeneously increased temperature along the slip surface within several seconds (Lavallée et al., 2012) suggests that the melting occurs under non-equilibrium conditions. Those estimated melting temperatures of minerals under equilibrium conditions are likely to be the lowest bound in our case. Therefore, we listed the matrix viscosity calculated with the temperatures ranged from 1500 °C to 1700 °C (Fig. 8 and Table 2). The matrix viscosity, though varied with different temperatures, is similar during the slip strengthening (Table 2). In addition, the heating rate of HVRFE under similar experimental conditions was estimated as ~130 °C per meter of slip (Lavallée et al., 2012), and the long duration of heating of LHVR037 was expected to achieve higher temperature than the shorter one of LHVR032. It means that the viscosity of matrix in LHVR037 would be lower than the one of LHVR032 if temperatures play an important role in the changes of viscosity on frictional melts. Taken together, it seems that the variation of chemical composition of matrix viscosity is unlikely to result in slip strengthening behavior in the postmelting regime.

The presence of water can play an important role to reduce the viscosity of frictional melts. Ujiie et al. (2009) conducted HVRFE on argillite (clay-rich rocks) and suggested that an increase in the matrix viscosity was resulted from the dehydration of frictional melts. However, water solubility in melts is highly functioned of pressure. At higher pressure, vesicles are observed together with a volatile content of the glassy matrix (Boullier et al., 2001). In our case, although the presence of vesicles indicates that the glass is saturated with a fluid present in the vesicles (Fig. 4), the applied normal stress is low (1 MPa). On the basis of the determination of the micro-Raman analysis, it suggests that the extremely low content of water was possibly remained in the matrices of pseudotachylyte (Fig. 5). Similarity to experimentally formed melts from argillite, slip strengthening in our cases was presumably resulted from the extremely low content of water in the frictional melt layer. The precise information of water in the matrices of pseudotachylyte is still unknown, and additional experiments such as EPMA analysis are required for estimation of the total amount of fluid in the melt. It is notable that the highly viscous melts may tend to terminate slip during experiments, and presumably result in stick–slip behavior shown with the oscillation in the end of the experiment.

Our results suggest that slip strengthening was presumably resulted from low content of water of the frictional melt layer, assuming pure silicate melts display a Newtonian rheological behavior. However, similarity to our experimental formed pseudotachylyte, crystal-bearing melts can also exhibit a non-Newtonian behavior mainly depending on the solid fraction, shear rate, and particle shapes and sizes (Del Gaudio et al., 2013; Mueller et al., 2010). A suspension of spherical particles in nano-scale sizes, like ultrafine spherical quartz grains in frictional melts in this study, would result in low viscosity of melts (Del Gaudio et al., 2013). Given the experimental observation at which it may be formed, the rheological behavior of pseudotachylyte with USQ remains largely unknown, and systematic works of HVRFE on various types of sedimentary rocks will be required in the future.

4.3. Implications for determining the latest slip zone and seismic slip in active faults hosted in sedimentary rocks at shallow crustal conditions

In TCDP case, ultrafine spherical quartz grains can be successfully generated on siltstone from both HVRFE (at a normal stress of 1 MPa and displacement of dozens of meters in this study) and comminution (6 h of milling in Hirono et al., 2014). The ultrafine spherical quartz grains, generated by comminution, are found to be covered with amorphous surface layer and can be evident for the broad bump in the XRD obtained from TCDP-B (Hirono et al., 2008b, 2014). In the other hand, the ultrafine spherical quartz grains, generated by HVRFE, are found in a frictional melt layer and in accordance with the characteristics of the PSZ obtained from TCDP-A (Kuo et al., 2009, 2011, 2014a). Given the experimental conditions at which it may be formed, the specific conditions for the formation of ultrafine spherical quartz of TCDP are still uncertain,

Table 2
Summary of mechanical and textural data for determining melt viscosity by HVRFE on siltstone.

	Shear stress (MPa)	thickness of melt layer (mm)	Apparent viscosity (Pa s)	Melt viscosity (corrected with clasts) (Pa s)	Clast content (vol.%)	Matrix viscosity (calculated with chemistry) (Pa s)		
						1500 °C	1600 °C	1700 °C
LHVR032	0.13	0.6	60	3	40	49	16	6
LHVR037	1.03	0.5	395	69	30	43	14	5

even if ultrafine spherical quartz grains were shown to be formed frictionally. However, it is reasonable to think that multi-fault zone processes (frictional heating and comminution) can occur simultaneously during earthquakes because of heterogeneous physical properties and geometry along the Chelungpu fault. Ultrafine spherical quartz particles have high solubility and might dissolve into interstitial fluid during the seismic cycle (Dove and Rimstidt, 1994). In addition, the ultrafine spherical quartz of 100 nm in size takes more than 3000 years to grow double in size (Sammis and Ben-Zion, 2008). The physical and chemical properties of the ultrafine spherical quartz documented by the researches indicate that regardless of the mode of formation, the ultrafine quartz grains, once generated, are extremely difficult to preserve and gradually grow in the geological period of time. Therefore, they are also potentially important indicators for determining the slip zone of the most recent seismic event.

The HVRFE on siltstone reproduced the microstructures of natural pseudotachylyte of the TCDP-A, and exhibited the frictional behavior of slip strengthening. The slip strengthening is attributed to the viscous melts derived from the extremely low content of water. It suggests that viscous melts generated during the Chi-Chi earthquake may tend to terminate seismic slip at very shallow depths. However, as we mentioned above, multi-fault zone processes were occurred simultaneously during earthquakes, and one may result in fault lubrication such as thermal pressurization (Boullier et al., 2009). To assess the contribution of physical and chemical processes to shear resistance on slip surfaces, the physico-chemo-microstructural modeling constrained by natural observation and experimental data is required to improve our understanding of seismic fault slip in an active fault.

5. Conclusion

We conducted HVRFE at a slip rate of 1.3 m/s and a normal stress of 1 MPa. Experiments were conducted on siltstone as it is a presumable source rock contributed the PSZ of 1999 Chi-Chi earthquake. Combination of mechanical, chemical and microstructural results shows (1) initial slip weakening was related to the generation of low viscosity melt patches, (2) the evolution of shear stress in the postmelting regime was congruent with frictional melt rheology, and (3) the slip strengthening in the postmelting regime was presumably resulted from the extremely low content of water of the frictional melt. In particular, the state-of-art of in situ synchrotron analyses present that ultrafine spherical quartz grains (~10 nm to 50 nm) were formed in the experimental pseudotachylyte. Our observations confirm that the ultrafine spherical quartz grains formed in rock friction experiments do occur in the PSZ of the Chelungpu fault and, by extension, other exhumed fault zones hosted in sedimentary rocks. In addition, we surmise the ultrafine spherical quartz is plausibly presented in the latest slip zones of the Chelungpu fault, and further infer that the viscous melts may terminate seismic slips at shallow crustal conditions.

Acknowledgments

We thank the reviewer Anne-Marie Boullier and the editor Rob Govers for their positive and constructive comments. We also thank Haibing Li and Jialiang Si for thin section preparation, and Hsiu-Ching Hsiao for laboratory support. We thank Hwo-Shuenn Sheu for technical support for our in situ synchrotron XRD analysis work. All raw mechanical data and microstructural observation used in this study are available by contacting the corresponding author L.-W. Kuo (liweikuo@ncu.edu.tw). This work was supported by the Ministry of Science and Technology (MOST 104-2116-M-002-028 to J. Suppe, MOST 103-2116-M-002-014 to S.-R. Song), the National Taiwan University (103R104051 to J. Suppe) and the National Natural Science Foundation of China (41330211).

Appendix A. Supplementary data

Supplementary data to this article can be found online at http://dx.doi.org/10.1016/j.tecto.2015.09.008.

References

Boullier, A.M., Ohtani, T., Fujimoto, K., Ito, H., Dubois, M., 2001. Fluid inclusions in pseudotachylytes from the Nojima fault, Japan. J. Geophys. Res. 106, 21965–21977. http://dx.doi.org/10.1029/2000JB000043.

Boullier, A.M., Yeh, E.C., Boutareaud, S., Song, S.R., Tsai, C.H., 2009. Micro-scale anatomy of the 1999 Chi-Chi earthquake fault zone. Geochem. Geophys. Geosyst. 10 (3), Q03016.

Boutareaud, S., Boullier, A.-M., Andreani, M., Calugaru, D.-G., Beck, P., Song, S.-R., Shimamoto, T., 2010. Clay-clast aggregates in gouges: a new textural evidence for seismic faulting. J. Geophys. Res. 115, B02408. http://dx.doi.org/10.1029/2008JB006254.

Brantut, N., Schubnel, A., Rouzaud, J.-N., Brunet, F., Shimamoto, T., 2008. High-velocity frictional properties of a clay-bearing fault gouge and implications for earthquake mechanics. J. Geophys. Res. 113, B10401. http://dx.doi.org/10.1029/2007JB005551.

Chester, J.S., Chester, F.M., Kronenberg, A.K., 2005. Fracture surface energy of the Punchbowl fault, San Andreas system. Nature 437, 133–136.

Chou, Y.-M., Song, S.-R., Aubourg, C., Lee, T.-Q., Boullier, A.-M., Song, Y.-F., Yeh, E.-C., Kuo, L.-W., Wang, C.-Y., 2012a. An earthquake slip zone is a magnetic recorder. Geology http://dx.doi.org/10.1130/g32864.1.

Chou, Y.-M., Song, S.-R., Aubourg, C., Song, Y.-F., Boullier, A.-M., Lee, T.-Q., Evans, M., Yeh, E.-C., Chen, Y.-M., 2012b. Pyrite alteration and neoformed magnetic minerals in the fault zone of the Chi-Chi earthquake (Mw 7.6, 1999): evidence for frictional heating and co-seismic fluids. Geochem. Geophys. Geosyst. Q08002 http://dx.doi.org/10.1029/2012GC004120.

Del Gaudio, P., Ventura, G., Taddeucci, J., 2013. The effect of particle size on the rheology of liquid–solid mixtures with application to lava flows: results from analogue experiments. Geochem. Geophys. Geosyst. 14. http://dx.doi.org/10.1002/ggge20172.

Di Toro, G., Goldsby, D.L., Tullis, T.E., 2004. Friction falls towards zero in quartz rock as slip velocity approaches seismic rates. Nature 427, 436–439.

Di Toro, G., Hirose, T., Nielsen, S., Pennacchioni, G., Shimamoto, T., 2006. Natural and experimental evidence of melt lubrication of faults during earthquakes. Science 311, 647–649.

Di Toro, G., Pennacchioni, G., Nielsen, S., Eiichi, F., Geophysics, International, 2009. Pseudotachylytes and earthquake source mechanics. In: Fukuyama, E. (Ed.), International Geophysics 94. Academic Press, pp. 87–133.

Di Toro, G., Mittempergher, S., Ferri, F., F., T. M. Mitchell, G. and Pennacchioni, 2012. The contribution of structural geology, experimental rock deformation and numerical modelling to an improved understanding of the seismic cycle. Preface to the special volume "physico-chemical processes in seismic faults". J. Struct. Geol. 38, 3–10.

Dove, P.M., Rimstidt, J.D., 1994. Silica–water interactions. In: Heaney, P.J., Prewitt, C.T., Gibbs, G.V. (Eds.), Silica: Physical Behavior, Geochemistry, and Materials Applications, Rev. Mineral. 29, pp. 235–290 (Mineral. Soc. Am., Washington, D. C.)

Fluegel, A., Varshneya, A.K., Earl, D.A., Seward, T.P., Oksoy, D., 2004. Improved composition–property relations in silicate glasses, part I: viscosity, ceramic transactions, 170, melt chemistry, relaxation, and solidification kinetics of glasses. Proceedings of the 106th Annual Meeting of the American Ceramic Society, 2005, pp. 129–143.

Goldsby, D.L., Tullis, T.E., 2011. Flash heating leads to low frictional strength of crustal rocks at earthquake slip rates. Science 334, 216–218.

Han, R., Shimamoto, T., Hirose, T., Ree, J.-H., J. i. Ando, 2007. Ultralow friction of carbonate faults caused by thermal decomposition. Science 316 (5826), 878–881.

Han, R., Hirose, T., Shimamoto, T., 2010. Strong velocity weakening and powder lubrication of simulated carbon faults at seismic slip rates. J. Geophys. Res. 115, B03412. http://dx.doi.org/10.1029/2008JB006136.

Han, R., Hirose, T., Jeong, G.Y., Ando, J.-i., Mukoyoshi, H., 2014. Frictional melting of clayey gouge during seismic fault slip: experimental observation and implications. Geophys. Res. Lett. 41 (15). http://dx.doi.org/10.1002/2014GL061246.

Hirono, T., Lin, W., Yeh, E.C., Soh, W., Hashimoto, Y., Sone, H., Matsubayashi, O., Aoike, K., Ito, H., Kinoshita, M., Murayama, M., Song, S.R., Ma, K.F., Hung, J.H., Wang, C.Y., Tsai, Y.B., 2006a. High magnetic susceptibility of fault gouge within Taiwan Chelungpu fault: nondestructive continuous measurements of physical and chemical properties in fault rocks recovered from Hole B, TCDP. Geophys. Res. Lett. 33, L15303. http://dx.doi.org/10.1029/2006GL026133.

Hirono, T., Ikehara, M., Otsuki, K., Mishima, T., Sakaguchi, M., Soh, W., Omori, M., Lin, W., Yeh, E.C., Tanikawa, W., Wang, C.Y., 2006b. Evidence of frictional melting within disk-shaped black materials discovered from the Taiwan Chelungpu fault system. Geophys. Res. Lett. 33, L19311. http://dx.doi.org/10.1029/2006GL027329.

Hirono, T., Sakaguchi, M., Otsuki, K., Sone, H., Fujimoto, K., Mishima, T., Lin, W., Tanikawa, W., Tanimizu, M., Soh, W., Yeh, E.C., Song, S.R., 2008a. Characterization of slip zone associated with the 1999 Taiwan Chi-Chi earthquake: X-ray CT image analyses and microstructural observations of the Taiwan Chelungpu fault. Tectonophysics 449, 63–84.

Hirono, T., Fujimoto, K., Yokoyama, T., Hamada, Y., Tanikawa, W., Tadai, O., Mishima, T., Tanimizu, M., Lin, W., Soh, W., Song, S.R., 2008b. Clay mineral reactions caused by frictional heating during an earthquake: an example from the Taiwan Chelungpu fault. Geophys. Res. Lett. 35, L16303. http://dx.doi.org/10.1029/2008GL034476.

Hirono, T., Kameda, J., Kanda, H., Tanikawa, W., Ishikawa, T., 2014. Mineral assemblage anomalies in the slip zone of the 1999 Taiwan Chi-Chi earthquake: ultrafine particles preserved only in the latest slip zone. Geophys. Res. Lett. 41 (9). http://dx.doi.org/10.1002/2014GL059805.

Hirose, T., Shimamoto, T., 2003. Fractal dimension of molten surfaces as a possible parameter to infer the slip-weakening distance of faults from natural pseudotachylytes. J. Struct Geol. 25 (10), 1569–1574.
Hirose, T., Shimamoto, T., 2005. Slip-weakening distance of faults during frictional melting as inferred from experimental and natural pseudotachylytes. Bull. Seismol. Soc. Am. 95, 1666–1673.
Hung, J.-H., Wu, Y.-H., Yeh, E.-C., Wu, J.-C., TCDP scientific party, 2007. Subsurface structure, physical properties, and fault zone characteristics in the scientific drill holes of Taiwan Chelungpu-Fault Drilling Project. Terr. Atmos. Ocean. Sci. 18, 271–293.
Ishikawa, T., Tanimizu, M., Nagaishi, K., Matsuoka, J., Tadai, O., Sakaguchi, M., Hirono, T., Mishima, T., Tanikawa, W., Lin, W., Kikuta, H., Soh, W., Song, S.R., 2008. Coseismic fluid–rock interactions at high temperatures in the Chelungpu fault. Nat. Geosci. 1. http://dx.doi.org/10.1038/ngeo308.
Janssen, C., Wirth, R., Wenk, H.-R., Morales, L., Naumann, R., Kienast, M., Song, S.-R., Dresen, G., 2014. Faulting processes in active faults — evidences from TCDP and SAFOD drill core samples. J. Struct. Geol. 65, 100–116. http://dx.doi.org/10.1016/j.jsg.2014.04.004.
Kano, Y., Mori, J., Fujio, R., Ito, H., Yanagidani, T., Nakao, S., Ma, K.F., 2006. Heat signature on the Chelungpu fault associated with the 1999 Chi-Chi, Taiwan earthquake. Geophys. Res. Lett. 33, L14306. http://dx.doi.org/10.1029/ 2006GL026733.
Kitano, T., Kataoka, T., Shirota, T., 1981. An empirical equation of the relative viscosity of polymer melts filled with various inorganic fillers. Rheol. Acta 20, 207–209.
Koch, C.C., 1997. Synthesis of nanostructured materials by mechanical milling: problems and opportunities. Nanostruct. Mater. 9, 13–22. http://dx.doi.org/10.1016/s0965-9773(97)00014-7.
Kuo, L.-W., Song, S.-R., Yeh, E.-C., Chen, H.-F., 2009. Clay mineral anomalies in the fault zone of the Chelungpu Fault, Taiwan, and their implications. Geophys. Res. Lett. 36, L18306. http://dx.doi.org/10.1029/2009GL039269.
Kuo, L.-W., Song, S.-R., Huang, L., Yeh, E.-C., Chen, H.-F., 2011. Temperature estimates of coseismic heating in clay-rich fault gouges, the Chelungpu fault zones, Taiwan. Tectonophysics 502, 315–327.
Kuo, L.-W., Song, S.-R., Yeh, E.-C., Chen, H.-F., Si, J., 2012. Clay mineralogy and geochemistry investigations in the host rocks of the Chelungpu fault, Taiwan: implication for faulting mechanism. J. Asian Earth Sci. 59, 208–218.
Kuo, L.-W., Hsiao, H.-C., Song, S.-R., Sheu, H.-S., Suppe, J., 2014a. Coseismic thickness of principal slip zone from the Taiwan Chelungpu fault Drilling Project-A (TCDP-A) and correlated fracture energy. Tectonophysics 619–620, 29–35.
Kuo, L.-W.H., Li, S.A.F., Smith, G. Di, Toro, J., Suppe, S.-R., Song, S., Nielsen, H.-S. Sheu, Si, J., 2014b. Gouge graphitization and dynamic fault weakening during the 2008 Mw 7.9 Wenchuan earthquake. Geology 42, 47–50.
Lavallée, Y., Mitchell, T.M., Heap, M.J., Vasseur, J., Hess, K.-U., Hirose, T., Dingwell, D.B., 2012. Experimental generation of volcanic pseudotachylyte: constraining rheology. J. Struct. Geol. 38, 222–233.
Lee, J.C., Chen, Y.G., Sieh, K., Mueller, K., Chen, W.S., Chu, H.T., Chan, Y.C., Rubin, C., Yates, R., 2001. A vertical exposure of the 1999 surface rupture of the Chelungpu fault at Wufeng, western Taiwan: structural and paleoseismic implications for an active thrust fault. Bull. Seismol. Soc. Am. 91 (5), 914–929.
Lejeune, A.M., Bottinga, Y., Trull, T.W., Richet, P., 1999. Rheology of bubble-bearing magmas, Earth Planet. Sci. Lett. 166, 71–84.
Lin, A., Shimamoto, T., 1998. Selective melting processes as inferred from experimentally-generated pseudotachylytes. J. Asian Earth Sci. 16, 533–545.
Ma, K.F., Song, T.R.A., Lee, S.J., Wu, H.I., 2000. Spatial slip distribution of the September 20, 1999, Chi-Chi, Taiwan, earthquake, Mw 7.6 — inverted from teleseismic data. Geophys. Res. Lett. 27, 3417–3420.
Ma, K.F., Tanaka, H., Song, S.R., Wang, C.Y., Hung, J.H., Tsai, Y.B., Mori, J., Song, Y.F., Yeh, E.C., Soh, W., Sone, H., Kuo, L.W., Wu, H.Y., 2006. Slip zone and energetics of a large earthquake from the Taiwan Chelungpu-Fault Drilling Project. Nature 444, 473–476.
Mishima, T., Hirono, T., Soh, W., Song, S.R., 2006. Thermal history estimation of the Taiwan Chelungpu fault using rock-magnetic methods. Geophys. Res. Lett. 33, L23311.
Mishima, T., Hirono, T., Nakamura, N., Tanikawa, W., Soh, W., Song, S.R., 2009. Changes to magnetic minerals caused by frictional heating during the 1999 Taiwan Chi-Chi earthquake. Earth Planets Space 61, 797–801.
Mizoguchi, K., Takahashi, M., Tanikawa, W., Masuda, K., Song, S.-R., Soh, W., 2008. Frictional strength of fault gouge in Taiwan Chelungpu fault obtained from TCDP Hole B. Tectonophysics 460, 198–205.
Mueller, S., Llewellin, E.W., Mader, H.M., 2010. The rheology of suspensions of solid particles. Proc. R. Soc. A 466, 1471–2946. http://dx.doi.org/10.1098/rspa.2009.0445.
Niemeijer, A., Di Toro, G., Griffith, W.A., Bistacchi, A., Smith, S.A.F., Nielsen, S., 2012. Inferring earthquake physics and chemistry using an integrated field and laboratory approach. J. Struct. Geol. 39, 2–36.
Rice, J.R., 2006. Heating and weakening of faults during earthquake slip. J. Geophys. Res. 111, B05311. http://dx.doi.org/10.1029/2005JB004006.
Sammis, C.G., Ben-Zion, Y., 2008. Mechanics of grain size reduction in fault zones. J. Geophys. Res. 113, B02306. http://dx.doi.org/10.1029/2006JB004892.
Sibson, R.H., 1975. Generation of pseudotachylyte by ancient seismic faulting. Geophys. J. R. Astron. Soc. 43 (3), 775–794.
Siman-Tov, S., Aharonov, E., Sagy, A., Emmanuel, S., 2013. Nanograins form carbonate fault mirrors. Geology 41 (6), 703–706.
Sone, H., Yeh, E.C., Nakaya, T., Hung, J.H., Ma, K.F., Wang, C.Y., Song, S.R., Shimamoto, T., 2007. Mesoscopic structural observations of cores from the Chelungpu fault system, Taiwan Chelungpu-Fault Drilling Project Hole-A, Taiwan. Terr. Atmos. Ocean. Sci. 18, 359–377.
Song, S.R., Kuo, L.W., Yeh, E.C., Wang, C.Y., Hung, J.H., Ma, K.F., 2007a. Characteristics of the lithology, fault-related rocks and fault zone structures in the TCDP Hole-A. Terr. Atmos. Ocean. Sci. 18, 243–269.
Song, Y.-F., et al., 2007b. X-ray beamlines for structural studies at the NSRRC superconducting wavelength shifter. J. Synchrotron Radiat. 14, 320–325. http://dx.doi.org/10.1107/S0909049507021516.
Spray, J.G., 1987. Artificial generation of pseudotachylylte using friction welding apparatus: simulation of melting on a fault plane. J. Struct. Geol. 9 (1), 49–60.
Spray, J.G., 1993. Viscosity determinations of some frictionally generated silicate melts: Implications for fault zone rheology at high strain rates. J. Geophys. Res. 98, 8053–8068.
Tisato, N., Di Toro, G., De Rossi, N., Quaresimin, M., Candela, T., 2012. Experimental investigation of flash weakening in limestone. J. Struct. Geol. 38, 183–199. http://dx.doi.org/10.1016/j.jsg.2011.11.017.
Tsutsumi, A., Shimamoto, T., 1997. High-velocity frictional properties of gabbro. Geophys. Res. Lett. 24 (6). http://dx.doi.org/10.1029/97GL00503.
Ujiie, K., Tsutsumi, A., Fialko, Y., Yamaguchi, H., 2009. Experimental investigation of frictional melting of argillite at slip rates: implication for seismic slip in subduction–accretion complexes. J. Geophys. Res. 114, B04308. http://dx.doi.org/10.1029/2008JB006165.
Viti, C., 2011. Exploring fault rocks at the nanoscale. J. Struct. Geol. 33, 1715–1727. http://dx.doi.org/10.1016/j.jsg.2011.10.005.
Wilson, B., Dewers, T., Reches, Z., Brune, J., 2005. Particle size and energetics of gouge from earthquake rupture zones. Nature 434, 749–752. http://dx.doi.org/10.1038/nature03433.
Wu, H., Ma, K.F., Zoback, M., Boness, N., Ito, H., Hung, J., Hickman, S., 2007. Stress orientations of Taiwan Chelungpu-Fault Drilling Project (TCDP) hole-A as observed from geophysical logs. Geophys. Res. Lett. 34, L01303. http://dx.doi.org/10.1029/2006GL028050.
Wu, Y.-H., Yeh, E.-C., Dong, J.-J., Kuo, L.-W., Hsu, J.-Y., Hung, J.-H., 2008. Core-log integration studies in hole-A of Taiwan Chelungpu-Fault Drilling Project. Geophys. J. Int. 174, 949–965.
Yang, C.H., Yu, W.-L., Dong, J.-J., Kuo, C.-Y., Shimamoto, T., Lee, C.-T., Togo, T., Miyamoto, Y., 2014. Initiation, movement, and run-out of the giant Tsaoling landslide — what can we learn from a simple rigid block model and a velocity–displacement dependent friction law? Eng. Geol. 182, 158–181.
Yeh, E.C., Sone, H., Nakaya, T., Ian, K.H., Song, S.R., Hung, J.H., Lin, W., Hirono, T., Wang, C.Y., Ma, K.F., Soh, W., Kinoshita, M., 2007. Core description and characteristics of fault zones from the Hole-A of the Taiwan Chelungpu-Fault Drilling Project. Terr. Atmos. Ocean. Sci. 18, 327–357.
Yin, G.-C., Song, Y.-F., Tang, M.-T., Chen, F.-R., Liang, K.S., Duewer, F.W., Feser, M., Yun, W., Shieh, H.-P.D., 2006. 30 nm resolution X-ray imaging at 8 keV using third order diffraction of a zone plate lens objective in a transmission microscope. Appl. Phys. Lett. 89. http://dx.doi.org/10.1063/1.2397483.